Journal of Global Environment Engineering, Vol. 4, pp. 1–29, 1998

MODELING STUDY OF THE LONG RANGE TRANSPORT OF ACIDIC POLLUTANTS OVER EAST ASIA AND THE WEST PACIFIC OCEAN —SENSITIVITY OF ACID DEPOSITION TO SCAVENGING MODEL PARAMETERS AND EMISSION SOURCE DISTRIBUTION—

Toshihiro Kitada [1]
Masato Nishizawa [2]

Abstract

Long range transport/transformation/deposition of various trace chemical species has been simulated over east- and southeast-Asia and the west Pacific ocean during February and March, 1994. Emission sources in the simulation include the natural sources of NO_x due to lightning, soil microbial activity and biomass-burning, and of SO_x from volcano as well as anthropogenic sources of NO_x, SO_x and hydrocarbons; the anthropogenic NO_x sources also include aircraft emissions. Comparison of calculated concentrations with PEM-West-B (Pacific Exploratory Mission-West, Phase B) campaign data showed good agreement for O_3, SO_2 and hydrocarbons such as C_2H_4, C_2H_6 and C_3H_8, and acceptable for NO_x, HNO_3 and PAN. Furthermore, dry and wet depositions of both S and N compounds were calculated and the results are evaluated by comparing with observation in Japan area. Sensitivity analysis of deposition to the scavenging coefficients, such as pH value in rain, and source strength is presented. The pH value in rain was found to be very important in estimation of wet sulfur-deposition. Relative contribution of the emission sources in East Asia to the acid deposition over Japan are also estimated. Finally, effects of the estimated coal consumption in China in 2010 on sulfur- and nitrogen-depositions over East Asia were evaluated using model calculations.

KEYWORDS: *Semi-global-scale model, long range transport, acid deposition, sulfate, nitrate, PEM-West, East Asia*

1. Introduction

Increasing energy use in East Asia may cause major damage to the terrestrial eco-systems in the area. The US EIA (Energy Information Administration, 1997), for example, predicts coal consumption in China will be doubled by the year 2010 as compared with that in 1990. Thus, the future emissions of SO_x and NO_x associated with this energy use may distribute

1 D. Eng., Professor, Dept. of Ecological Eng., Toyohashi University of Technology, Tempaku-cyo, Toyohashi, 441-8580, Japan.
2 M. Eng., Doctoral Student, Graduate School of Environment and Life Engineering, Toyohashi University of Technology, Tempaku-cho, Toyohashi, 441-8580, Japan.

acidic pollutants widely over East Asia, and also may raise tropospheric O_3 concentration, resulting in possible global warming and increase of oxdizing potential of the atmosphere. NO_x and SO_x have also other natural and anthropogenic emission sources such as soil microbial activity, biomass burning, lightning and aircrafts crusing in lower stratosphere for NO_x, and active volcano and ocean for sulfur compounds. For effective management to preserve desirable atmospheric environment over a large area, such as control of loading to biosphere of potentially toxic air pollutants, a comprehensive modeling of transport/tranformation/deposition of trace chemical species is definitely required.

In this paper, a semi-global scale model, which can be used for the management of atmospheric environment, is briefly introduced, and to show the model's performnace the simulation results for March in 1994 are compared with the observation acquired during PEM West-B campaign. Furthermore, sensitivity of acidic deposition to model parameters such as pH in rain water and to emission source distribution and strength is discussed for Japan area. A cenario of doubled emission sources in China for 2010 is performed and its possible effects to East Asia are evaluated. Similar topics were discussed in previous studies (for example, Matsuoka, 1992, Murao *et al.*, 1993, and Ikeda and Higashino, 1997).

2. Semi-global Scale Transport/Chemistry/Deposition Model

2.1 Governing Equations

The semi-global scale model consists of a set of partial differential equations that account for advection, diffusion and chemical reactions of trace chemical species. The model also includes processes of vertical mass-transport by subgrid scale cumulus convection and wet- and dry-depositions. The previous version of this model was applied to east Asia and the northwestern Pacific ocean for the analysis of data from PEM West-A campaign (Kitada *et al.*, 1996 and 1998). The governing equations are as follows, where index for chemical species, i = 1, 2, ..., 38:

$$C\frac{\partial X_i}{\partial t} + CU\frac{\partial X_i}{\partial x} + CV\frac{\partial X_i}{\partial y} + C\dot{\sigma}\frac{\partial X_i}{\partial \sigma} = \frac{\partial}{\partial x}\left(CE_\phi\frac{\partial X_i}{\partial x}\right) + \frac{1}{cos\theta}\frac{\partial}{\partial y}\left(Ccos\theta E_\theta\frac{\partial X_i}{\partial y}\right) + \frac{\rho g^2}{\pi^2\, r^2}\frac{\partial}{\partial \sigma}\left(C\rho r^2 E_\sigma\frac{\partial X_i}{\partial \sigma}\right) + R_i \qquad (1)$$

where $dx = r\,\cos\theta\, d\phi$, $dy = r\, d\theta$, $\sigma = (P - P_T)/\pi$, $\pi = P_S - P_T$, $\dot{\sigma} = \{\left(\frac{\partial z}{\partial t}\right)_\sigma + \vec{V}\cdot\nabla_\sigma z - W\}\frac{\rho g}{\pi}$. X_i is the non-dimensional concentration of the i^{th} chemical species; ρ the air density in kg m^{-3}; C the air density in kmol m^{-3}; θ and ϕ denote latitude and longitude, respectively; r is the distance from the center of the Earth (approximated by the averaged radius of the earth); P_S and P_T denote the atmospheric pressures at the earth's surface and the top boundary, respectively: P_T is set at 10 hPa; z is the altitude of a σ-surface; U and V are the horizontal wind velocities for ϕ and θ directions, respectively; W is the vertical wind velocity; g is the gravitational acceleration; E_ϕ and E_θ denotes horizontal eddy diffusivity; and E_σ denotes vertical eddy diffusivity and R_i represents the chemical reaction term for the i^{th} species. Here, $E_\phi = E_\theta = 0.02(r\,\triangle\theta)^2\sqrt{D_T^2 + D_S^2}$, where $D_T = \left(\frac{\partial U}{\partial \phi} - \frac{\partial (V cos\theta)}{\partial \theta}\right)\frac{1}{r\cos\theta}$ and $D_s = \left(\frac{\partial V}{\partial \phi} + \frac{\partial (U\cos\theta)}{\partial \theta}\right)\frac{1}{r\cos\theta}$, have been used (Washington and Williamson, 1977).To

determine the vertical diffusivity E_σ in the atmospheric boundary layer (*i.e.*, ABL), outputs from a $k-\epsilon$ turbulence model for ABL (Kitada, 1987) has been used.The reaction terms, R_i, accounts for 25 advected species (NO, NO_2, HNO_3, PAN, $RONO_2$, HNO_2, NO_3, N_2O_5, HNO_4, CO, SO_2, SO_4^{2-}, O_3, H_2O_2, CH_4, C_2H_6, C_3H_8, C_2H_4, ALKENEs, HCHO, ALDEHYDEs, HCOOH, ACETIC ACID, ROOH, and LUMPED KETONEs) and 13 species assumed to be in quasi-steady state (*e.g.*, OH, HO_2,...,etc.), forming a system of 90 chemical reactions (an adaptation from the model in Lurmann *et al.*, 1986).

2.2 Dry and Wet Deposition Processes

Dry deposition onto the earth's surface was expressed using the dry deposition velocity. Chemical species subjected to the dry deposition were SO_2, SO_4^{2-}, NO_2, HNO_3, H_2O_2, O_3, PAN, HCHO, HCOOH, etc. Typical velocity values used in the simulations were, for example, 0.5 cms^{-1} for land surface and 0.1 cms^{-1} for sea surface for SO_2; 0.1 cms^{-1} for both land and sea surfaces for SO_4^{2-}; and 0.5 cms^{-1} for land surface and 0.3 cms^{-1} for sea surface for HNO_3.

For wet removal processes, semi-empirical equations were used for SO_2, SO_4^{2-}, HNO_3, and H_2O_2; the equations were derived on the basis of capture of aerosol particle by cloud and rain drops and gas absorption into the rain drops (Kitada, 1994). Meteorological parameters used in the wet deposition equation were the height of cloud-top, and precipitation intensity. Scavenging coefficients of sulfate and nitrate particles by rain and snow were expressed as follows:

For rain,

$$\Lambda_{p,rain} = 6 \times 10^{-4} \eta_r P^{0.75} \tag{2}$$

where $\Lambda_{p,rain}$ denotes the scavenging coefficient for particle due to rain in s^{-1}, η_r the collection efficiency of aerosol by rain and was assumed to be $0.3 \sim 0.5$, and P the precipitation intensity in $mmhr^{-1}$.

For snow, following Slinn (1974),

$$\Lambda_{p,snow} = \frac{\rho_w g \eta_s (3.6 \times 10^{-6} P)}{\rho_a V_t^2} \tag{3}$$

where ρ_w denotes the density of water (= 1000 kgm^{-3}), g the gravitational acceralation (= 9.8 ms^{-2}), ρ_a the air density ($\sim$ 1 kg m^{-3}), V_t the average settling velocity of the snow flakes in ms^{-1} and is expressed by the following equation recommended by Knutson *et al.* (1976):

$$V_t = (102 + 51 \log_{10} d_c)/100 \tag{4}$$

where d_c denotes the diameter of the circle circumscribed about the average snowflake in cm. $\Lambda_{p,snow}$ in Eq.(3) was approximated as 5.6×10^{-4}P by assuming d_c=500μm and η_s=0.002 (judged from figure in Slinn, 1977).

Coefficients (s^{-1}) for scavenging, due to rain, of gaseous species were given in the model, for example, for SO_2,

$$\Lambda_{SO2} = \beta \frac{\alpha P}{3.6H} \tag{5}$$

$$\alpha = 10^{-6} R T H_{eff,SO_2} \tag{6}$$

where H denotes the height of cloud-top in m, R the universal gas constant (=0.082ℓ atm K^{-1} mol^{-1}), T the air temperature in K, and H_{eff,SO_2} the inverse of the effective Henry's law

constant for SO_2 in mole ℓ^{-1} atm^{-1}, which is a function of the hydrogen ion concentration in rain drop, and is defined as:

$$H_{eff,SO_2} = K_1 \left(1 + \frac{K_2}{[H^+]} + \frac{K_2 K_3}{[H^+]^2} \right) \tag{7}$$

where K_1, K_2, and K_3 are equilibrium constants of the following reactions with concentrations in atm and M:

$$SO_2(g) \rightleftharpoons SO_2(\ell) \ : \ K_1 = 1.23 \exp\left[3120\left(\frac{1}{T} - \frac{1}{298}\right)\right]$$

$$SO_2(\ell) \rightleftharpoons H^+ + HSO_3^- \ : \ K_2 = 1.23 \times 10^{-2} \exp\left[1960\left(\frac{1}{T} - \frac{1}{298}\right)\right]$$

$$HSO_3^- \rightleftharpoons H^+ + SO_3^{2-} \ : \ K_3 = 6.61 \times 10^{-8} \exp\left[1500\left(\frac{1}{T} - \frac{1}{298}\right)\right]$$

For absorption of HNO_3,

$$H_{eff,HNO_3} = \frac{K_4}{[H^+]} \tag{8}$$

where K_4 denotes equilibrium constant for

$$HNO_3(g) \rightleftharpoons H^+ + NO_3^- \ : \ K_4 = 2.6 \times 10^6 \exp\left[8700\left(\frac{1}{T} - \frac{1}{298}\right)\right]$$

For example, the estimated value of α is 0.671 for pH = 5.6 at 273 K, 0.330 for pH = 5.3 at 273 K and 0.089 for pH = 5.0 at 298 K. Equation (5) has been derived by assuming that S(IV) concentration in precipitation can be expressed with the hypothetical concentration of S(IV), which is in equilibrium with the atmospheric SO_2 concentration averaged over the height from ground to cloud-top. The factor β in Eq.(5) is an "equilibrium index" and represents the ratio of the real S(IV)- to the hypothetical equilibrium S(IV)-concentrations in precipitation, and was assumed unity for the SO_2,-S(IV) system. Expression similar to Eq. (5) was used also for HNO_3 and H_2O_2, where the "equilibrium" ratio β was given as 0.38×10^{-8} for HNO_3 and 0.055 for H_2O_2; these values were determined by a series of numerical experiments in which temporal development of various chemical species in a water drop, falling through pollutants-containing-atmosphere, was calculated using a sub-module of a comprehensive acid rain model described in Kitada *et al.* (1993a,b). The scavenging coefficients Λ in Eqs. (2), (3), and (5) were used in the following first order removal equation, which was incorporated into the model:

$$\frac{\partial CX_i}{\partial t} = -\Lambda CX_i \tag{9}$$

2.3 Vertical Mass Transport in Sub-grid Scale

Vertical mass transport due to sub-grid scale cumulus convection was included in the model. Height of the cumulus convection and the cloud air mass subjected to the convection were determined using vertical profile of water vapor and resolvable scale vertical wind velocity of input meteorological data (*i.e.*, ECMWF data). In vertical column, from the earth's surface to top boundary, with 2.5° × 2.5° horizontal cross section, the following conditions were applied

for the cumulus convection process evoked : (1) relative humidity to be larger than 80 % at the top of cumulus convection ; (2) relative humidity larger than 60 % within the cumulus convection ; and vertical wind at the fourth vertical grid, *i.e.* height of around 1 km, to be upward. Horizontal area ratio q the cumulus convection was assumed 0.1 within one grid cell. The assumptions made for the process, which are similar to those used in Strand and Hov (1993), were: (1) cumulus convection draws air mass out of boundary layer (*i.e.*, approximately below 1 km high above ground) and then redistributes it to upper layers; (2) continuity of air mass is maintained within a column over each horizontal grid cell; and (3) the compensating subsidence occurs from one layer to the one below.

3. Meteorological Inputs, Emission Sources and Simulation Cases

3.1 Meteorological data

For input meteorological fields of air flow, temperature, humidity and pressure, the ECMWF basic consolidated data set was used. The original data has longitudinal and latitudinal resolutions of 2.5 degree, and time resolution of 12 hours, and is defined at 15 vertical layers from the earth's surface to 10 hPa. These meteorological data were interpolated and modified vertically so that the data give information at 17 grid points in σ coordinate, where two additional vertical grid points are set for atmospheric boundary layer. The data are also temporally interpolated with 30 minutes interval for the simulation. Diurnal variation of boundary layer activity was modelled using the outputs of a k-ϵ model (Kitada, 1987 and Kitada *et al.*, 1998). Precipitation fields were taken from the NCAR archive of the monthly values (Xie and Arkin, 1995) with limited modification using observation data in Japan area. The monthly precipitation was distributed over the monthly cumulus convection events and the cases at any height when relative humidity exceeded 90 % at any height within the vertical air column.Figure 1 shows precipitation field in March, 1994.

3.2 Emission sources

Five types of NO_x emission sources are considered in the present study: (1) source distribution due to fuel combustion at surface level is shown in Fig. 2a, where the original $1° \times 1°$ distribution by Akimoto and Narita (1994) was converted into $2.5° \times 2.5°$ distribution; (2) NO_x emission due to soil microbial activity in March is displayed in Fig. 2b, which was also adapted from that by Yienger and Levy (1995); (3) NO lightning emission is shown in Fig. 2c which was estimated from that by Kumar *et al.* (1995) taking its vertical profile (Feichter and Crutzen, 1990) into account; (4) aircraft NO_x emission was taken from the UADP (NASA Langley Research Center, 1997); (5) biomass burning NO_x emission was tentatively assumed to have the same distribution as the soil NO_x emission; and (6) seasonal variations in emission sources of fuel combustion were considered using GEIA data (GEIA Data Management and Communication Center, 1997). Table 1 lists source strength of various NO_x emissions in calculation domain (see, for example, Fig. 2a for the calculation domain). Non methane hydrocarbons were grouped into C_2H_6 (ethane), C_3H_8 for propane and benzene, C_2H_4 (ethene) and ALKE for $\geq C_3$ alkenes. Emissions for these species were determined so as to be proportional to the NO_x emissions by fuel combustion, aircraft emission, and biomass-burning. The proportional coefficients were estimated using data in Aichi Prefecture, Japan (Nakanishi,1996)

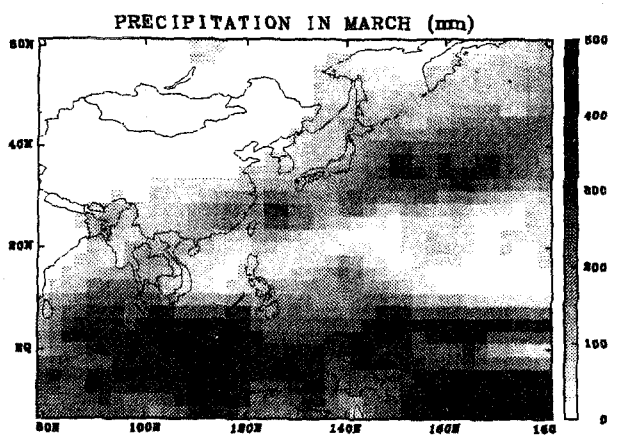

Figure 1. Precipitation in March, 1994 in mm month^{-1}.

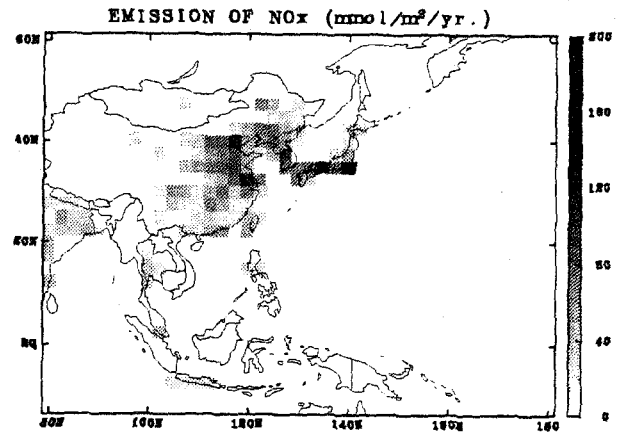

(a)

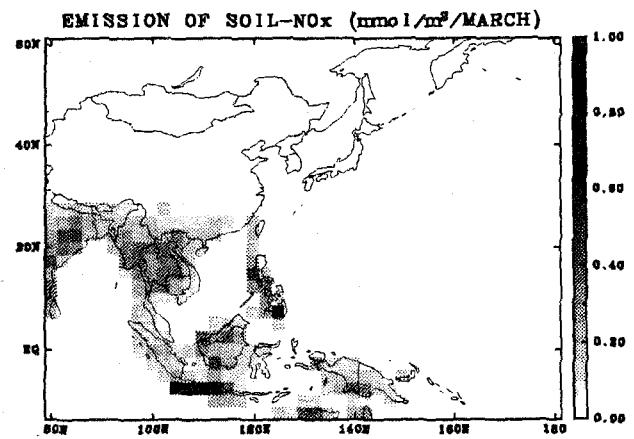

(b)

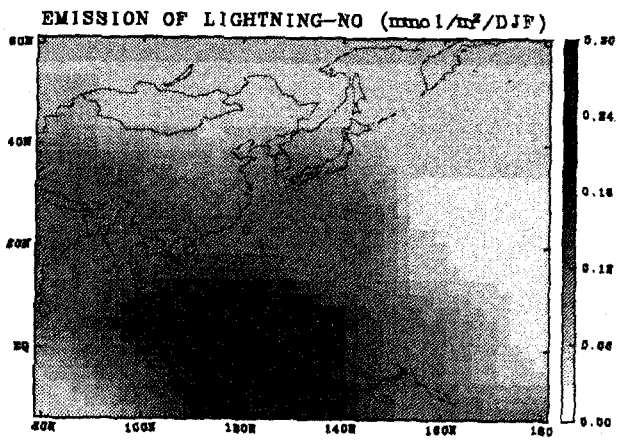

(c)

Figure 2. *Spatial distribution* of NOx emission sources in mmol m^{-2}yr^{-1}. (a) fuel combustion in 1987 (Akimoto and Narita, 1994).(b) soil microbial activity in March, 1990 (Yienger and Levy II, 1995), and (c) *NO* emission, within vertical column, by lightning during 3 months from Dec., 1979 to Feb., 1980 (Kumar et al., 1995). DJF denots December, January, and February.

Table 1. NO_x emissions in calculation domain for the BASE case (Table 2).

Source Type	Emission Strength*	Relative Strength
Fuel Combustion‡	3.59×10^8	1
Aircraft§	5.79×10^6	0.016
Lightning†	3.40×10^7	0.097
Soil‡	3.87×10^7	0.108
Biomass Burning$	3.87×10^7	0.108

* (kgN month^{-1}) ; ‡ Akimoto & Narita (1994) ;
§ NASA Langley (1997) ; † Kumar *et al.* (1995) ;
‡ Yienger and Levy (1995) ; $ assumed.

as follows: 0.25 for C_2H_6, 0.45 for C_3H_8, 0.4 for C_2H_4, and 0.2 for ALKE when NO_x emission on molar basis is assumed to be 1. Methane emissions were collected from the work by Matthews and Fung (1987) and Lerner *et al.* (1988). SO_2 emission due to fuel combustion was again adapted from that by Akimoto and Narita (1994), and that from volcano, in which only Mt. Sakurajima was considered, was assumed to be 5.0×10^5 ton-SO_2 yr^{-1} or 3.0×10^5 kmol (14-day)$^{-1}$ (see Table 3).

3.3 Simulation domain and simulation cases

The simulation domain was 80 °E ~ 180°E and 12.5°S ~ 60°N, with grid size of 2.5 degree for horizontal directions. In the vertical direction, 17 variable grids were used. Time step was 30 minutes for transport calculation and 12 seconds for chemistry. Appropriate minimum background concentrations, which were estimated from PEM West-B data, were assumed for all species throughout the entire simulation domain and period. For the initial ozone profile, climatological distribution in Fishman and Crutzen (1978) was used. The simulated time was from 00GMT on 21 Feb. to 00GMT on 15 March, 1994. At the top boundary, the concentrations were fixed mostly at their initial values. At the side boundaries, zero horizontal gradients of the concentrations were applied for outflow case, while prescribed advective fluxes were specified for inflow case, prexcribed fluxes which were estimated using the concentrations at previous time step and wind velocity on the boundaries.

Several simulations were performed to see the effect on acidic depositions of the parameters related to scavenging of pollutants by hydrometeors and the strength of anthropogenic emission sources. Table 2 summarizes these simulation cases. Base case uses following conditions: (i) $\eta_r = 0.5$ in Eq.(2) and $\eta_s = 0.002$ in Eq.(3), (ii) pH value in rain was assumed to be 5.6 in Eq. (6); for example, at T=273 K in this case, $\alpha = 0.671$ for SO_2, and 3.36×10^8 for HNO_3; the "equilibrium index" β was assumed to be 1, 0.36×10^{-8}, and 0.055 for SO_2, HNO_3, and H_2O_2, respectively, (iii) dry deposition velocity in m s^{-1}: SO_2 (0.005 for land, 0.001 for sea), SO_4^{2-} (0.001 for both land and sea), HNO_3 (0.005 for land, 0.003 for sea), NO_2 (0.002 for land, 0.00001 for sea), and PAN (0.0005 for land, 0.0005 for sea), and (iv) annually averaged emission sources.

4. Results and Discussion

4.1 Comparison between Calculated and Observed Concentrations

During the first two weeks in March, the PEM West-B campaign launched six missions over Japan area, *i.e.* Flight 13 to 18. Here we will discuss results from Flight 15, which left Yokota Base at 23:30GMT on 5 March (*i.e.* 08:30JST on 6 March; JST, Japanese Standard Time) and returned at 07:00GMT (*i.e.* 16:00JST) on 6 March. Figure 3a shows the surface weather chart at 00GMT (*i.e.* 09JST) on 6 March, and Fig. 3b the route of Flight 15. Figure 3a indicates that the Japan area was under a typical winter weather system, *i.e.* an anticyclone was over the western part of the Sea of Japan with a cyclone over the northern Sea of Okhotsk. Stably stratified layer associated with the anticyclone, thus, existed over and around the Japanese islands at relatively low altitudes such as 2 km over the Sea of Japan and 3 km over the Pacific Ocean according to the temperature profile observed during the flight, though it was cloudy and weakly snowing below the stable layer on the Japan Sea side of the islands.

Figure 4 compares calculated concentrations (BASE, Table 2) with the observed along the flight route (see Fig. 3b): (a) NO, (b) HNO_3, (c) C_2H_4, (d) O_3, (e) SO_2, and (f) SO_4^{2-}; in Fig. 4, open circles (○) denote the BASE case, "plus" symbols the observed data, and solid lines without symbol indicate the flight height which varied from 300 m to 11 km. Figure 4 demonstrates that the calculated concentrations well simulate those observed. It can be found in Fig. 4 that there are two clear peaks in both of observed and calculated concentrations of NO, C_2H_4, SO_2, and SO_4^{2-}, which represent chemical species with anthropogenic emission sources at surface or those chemically produced from the primary pollutants; the first peak around 01 and 02 GMT on 6 March was observed in the boundary layer over the Sea of Japan, and the second peak around 05 GMT also in the boundary layer over the Pacific Ocean, thus indicating the first peak was largely affected by the continental sources and the second peak similarly by both continental and Japanese sources. Observed HNO_3 in Fig. 4b does not show so remarkable peaks as SO_4^{2-} (see Fig. 4f). One reason for this may be that the observed HNO_3 represents only gaseous nitric acid and does not include particulate nitrate, while the model calculated HNO_3 includes both gaseous and particulate nitrate.

The O_3 concentration in Fig. 4d also has two peaks, but in contrast to other chemical species those peaks were observed at altitudes of about 9 km when the airplane was flying in lower stratosphere, indicating influence of stratospheric air mass. As a whole, it can be seen that both of the observed and the calculated concentrations for all chemical species except for O_3 tend to be high/low, when the flight height is low/high; among the chemical species, only O_3 does not have its direct source at the earth's surface. These indicate that there was no significant exchange of air mass between boundary layer and upper troposphere over Japan area; suggesting that the exchange of air mass was suppressed by the stably stratified layer associated with the above-mentioned synoptic-scale weather condition, *i.e.*, temperature inversion at and above the top of anticyclone which consists of relatively shallow cold air mass formed by radiative cooling in Siberia.

4.2 Spatial distributions of the depositions of N- and S-compounds

Characteristics of the spatial distributions of acid depositions in east Asia will be discussed in this subsection based on the simulation results of the base case (BASE) and the background case (EMI_BACK) in Table 2.

Figures 5a and b show the BASE case results of the "total" dry- plus wet-depositions of N- and S-compounds accumulated for 14 days from 00GMT on 1 March to 00GMT on 15 March,

Table 2. Simulation cases.

Case	Description
BASE	Base case($\eta_r = 0.5$ in Eq. (2); $\eta_s = 0.002$ in Eq. (3); pH in rain = 5.6; dry deposition velocity for land, 0.5 cm/s for both HNO_3 and SO_2; annually averaged emission sources).
PH5	Same as BASE but for pH in rain=5.0.
PH5.3	Same as BASE but for pH in rain=5.3.
ETAR3	Same as BASE but for $\eta_r = 0.3$.
ETAS1	Same as BASE but for $\eta_s = 0.001$.
DRYVE	Same as BASE but for dry deposition velocity for land, 0.3 cm/s for both HNO_3 and SO_2.
EMI_DJF	Same as BASE but for emissions* multiplied by factors for winter (GEIA, 1997).
EMI_DJF	Same as EMI_DJF but for doubled emissions* in China.
EMI_MAM	Same as BASE but for emissions* multiplied by factors for spring (GEIA, 1997).
EMI_JPOFF	Same as BASE but for Japanese emissions♯ off.
EMI_BACK	Same as BASE but for all emissions* off except for SO_2 from volcano.

* emissions due to fuel combustion.
♯ all emissions.

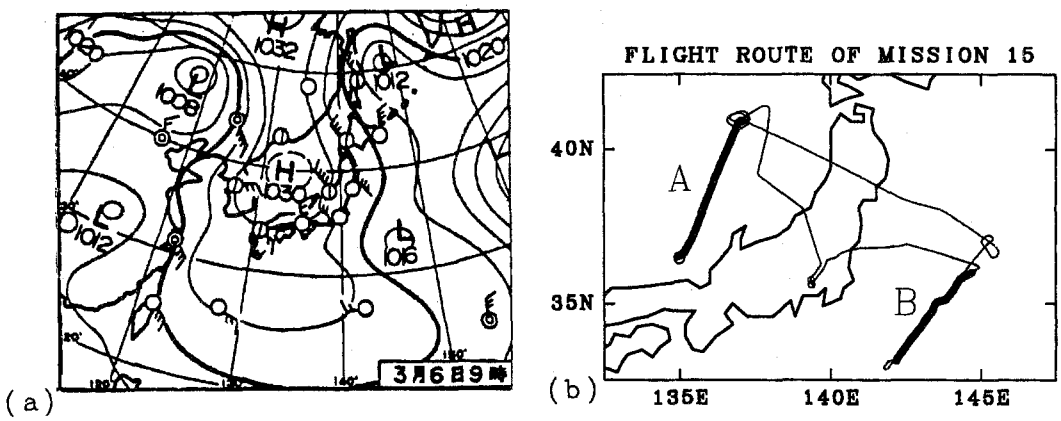

Figure 3. (a) Surface weather chart for East Asia at 00 GMT on 6 March, 1994 ; (b) Flight route of Mission 15 on 6 March, 1994 (PEM-WEST : B). Bold lines A and B indicate that the flight height was 300m high or less : A for 2 to 3 GMT and B for 5 to 6 GMT (see Fig. 4).

in mmol $m^{-2}(14day)^{-1}$, respectively. N-compounds means $HNO_3(NO_3^-)$, NO_2, and PAN for dry deposition, but only $HNO_3(NO_3^-)$ for wet deposition, while S-compounds stand for SO_2 and SO_4^{2-} for both dry and wet depositions. The "total" deposition includes those due to background concentrations, which were assumed, using PEM-B observation, to be 50, 25, and 10 pptv for HNO_3, SO_2, and SO_4^{2-} in the troposphere, respectively. These background values can be considered as baseline contributions from outside of the calculation domain, and also the contribution from ocean emission in case of S-deposition. Here N-compound stands for HNO_3 (including NO_3^-), and S-compound for SO_2 and SO_4^{2-}. Both N- and S-depositions in Fig. 5 indicate extremely large values in and near anthropogenic emission source areas. However, some difference between N- and S-depositions can be found, *i.e.* N-deposition in Japan area is relatively large compared with that in China area, which is different from S-deposition (Fig. 5b) and apparently reflects larger relative strength of Japanese NO_x emissions; the ratio of Japanese emission to Chinese is 0.24 for NO_x and about 0.05 for SO_x in 1987.

Wet depositions in Figs. 6a and b show similar tendency to those in Figs. 5a and b, *i.e.* dry + wet depositions. It may be noteworthy that the calculated wet N-deposition in Fig. 6a suggests possible large N-depositions in wide tropical southeast Asia caused by the NO_x sources of soil-microbial activity and lightning. Deposition due to the "background" HNO_3, SO_4^{2-}, and SO_2 concentrations were evaluated as in Figs. 7a and b, where the contributions of the background- to total-depositions are expressed in %. Figure 7 suggests: (1) the contribution of "background" deposition may be less than 10 % in China and Japan emission source area in both N- and S-depositions, and (2) judging from the large area covered by 10 and 20 % lines in Fig. 7b, the deposition of sulfur compounds in the area is largely dominated by the anthropogenic sources. Small circle of 20 % contour line over Kyusyu Island, Japan reflects effect of natural sulfur emission from a volcano, Mt. Sakurajima. (3) In the tropical southeast Asia such as Java and Sumatra islands and Malay peninsula, 30 to 40 % of N-deposition are attributable to background deposition.

Although there have been few observational studies on acid deposition in southeast Asia, Bruijinzeel(1989) reports the concentarations of SO_4^{2-} and NO_3^- in precipitations in south- and mid-Java island, Indonesia, averaged over 18 months of the three years from 1975 to 1978, were 4.8 and 4.3 μ eq ℓ^{-1}, respectively, with its precipitation of 4670 mm yr^{-1}. These concentrations with the precipitaton allow the estimation of the wet depositions of NO_3^- as 20.1 mmol $m^{-2}yr^{-1}$, *i.e.* 0.77 mmol $m^{-2}(14day)^{-1}$, and those of SO_4^{2-} as 11.2 mmol $m^{-2}yr^{-1}$, *i.e.* 0.43 mmol $m^{-2}(14day)^{-1}$. Though straightforward comparison of the simulation-derived depositions with these observation-derived is impossible, the calculated depositions shown in Fig. 6a and b, *i.e.* the wet deposition of $HNO_3(NO_3^-)$ larger than 0.5 and that of SO_4^{2-} larger than 0.2 in mmol $m^{-2}(14day)^{-1}$ agree qualtatively with the observation-derived. However, other study which looked at concentration of ions in precipitation over Jakarta area shows much higher SO_4^{2-} concentrations such as 49 μ eq ℓ^{-1} (Gillett *et al.*, 1992). Further study is definitely needed on acid depostions in the southeast Asia.

4.3 Comparison of N- and S-depositions between observed and calculated over Japan area

Calculated depositions were compared with observed data (listed in Suuri Keikaku Co., 1997) as 14 days accumulated depositions over Japan area; the fourteen days stand for a period from 00GMT on 1 March to 00GMT on 15 March, 1994. Apparently, the samples for wet and dry depositions (Suuri Keikaku, Co., 1997) were collected using an autosampler, which opens its mouth for wet deposition according to precipitation-sensor, but collects dry-deposition

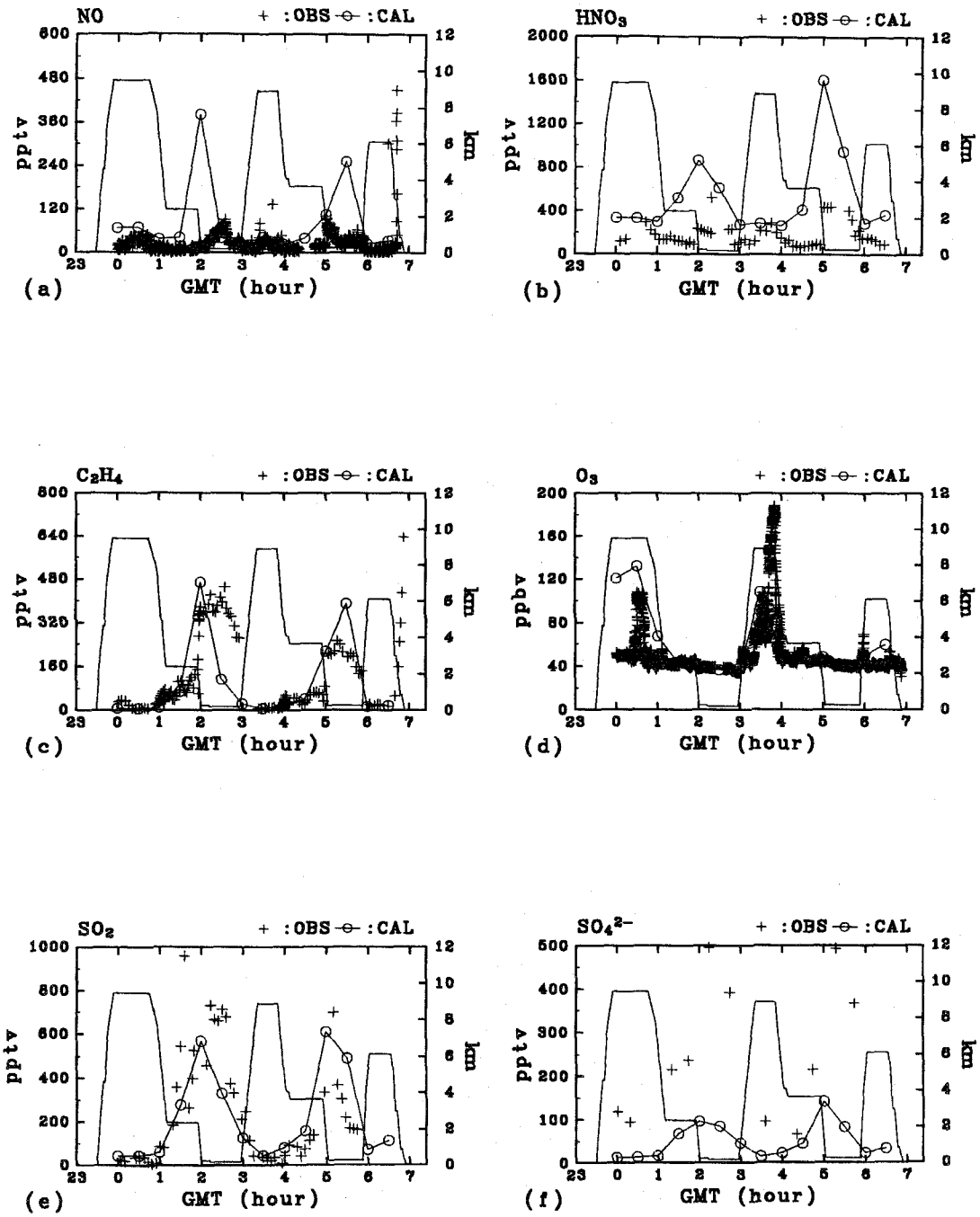

Figure 4. Comparison of the calculated concentrations (BASE in Table 2) with the observed along Mission 15 flight route : (a) NO, (b) HNO_3, (c) C_2H_4, (d) O_3, (e) SO_2, and (f) SO_4^{2-}.

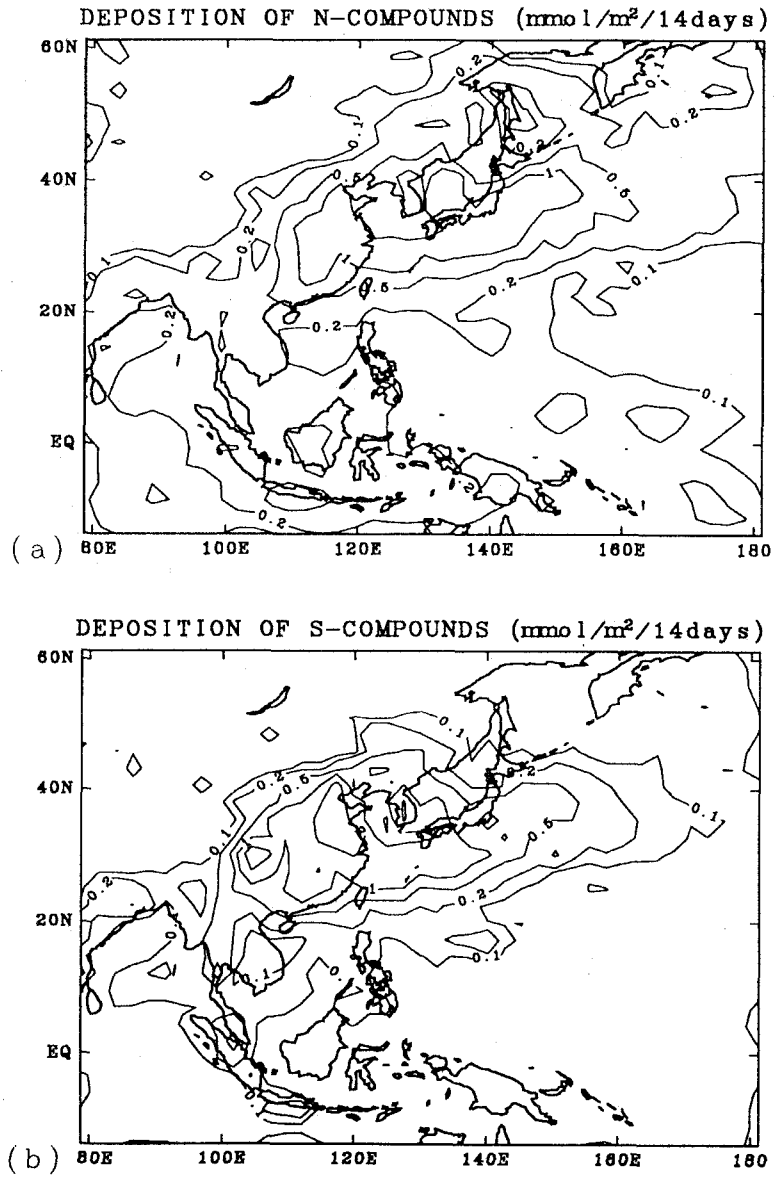

Figure 5. Calculated dry + wet deposition (BASE) of (a) N- and (b) S-compounds in mmol m^{-2} $(14day)^{-1}$. The fourteen day stands for the period from 00GMT, 1 March to 00GMT, 15 March, 1994. Contour lines : 0.1, 0.2, 0.5, 1, and 2.

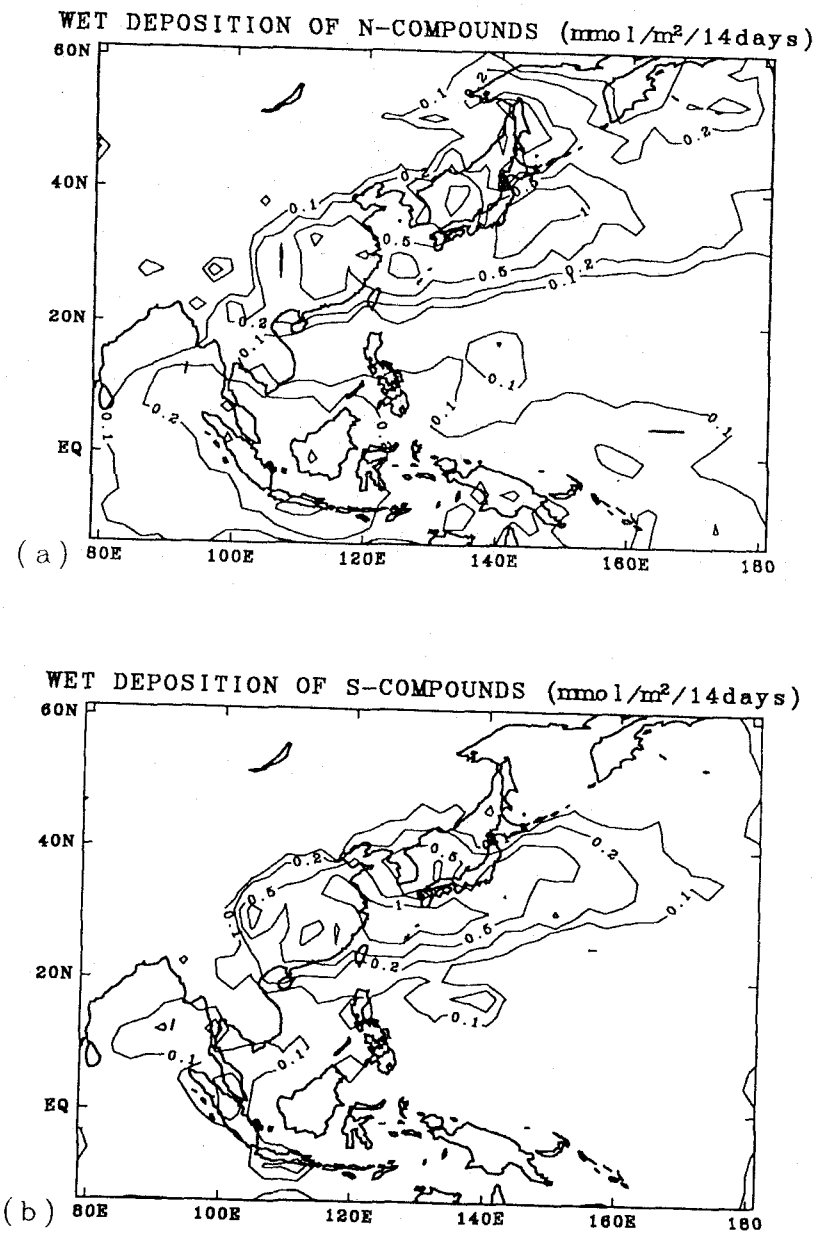

Figure 6. Same as in Fig. 5 but for wet deposition : (a) N- and (b) S-compounds.

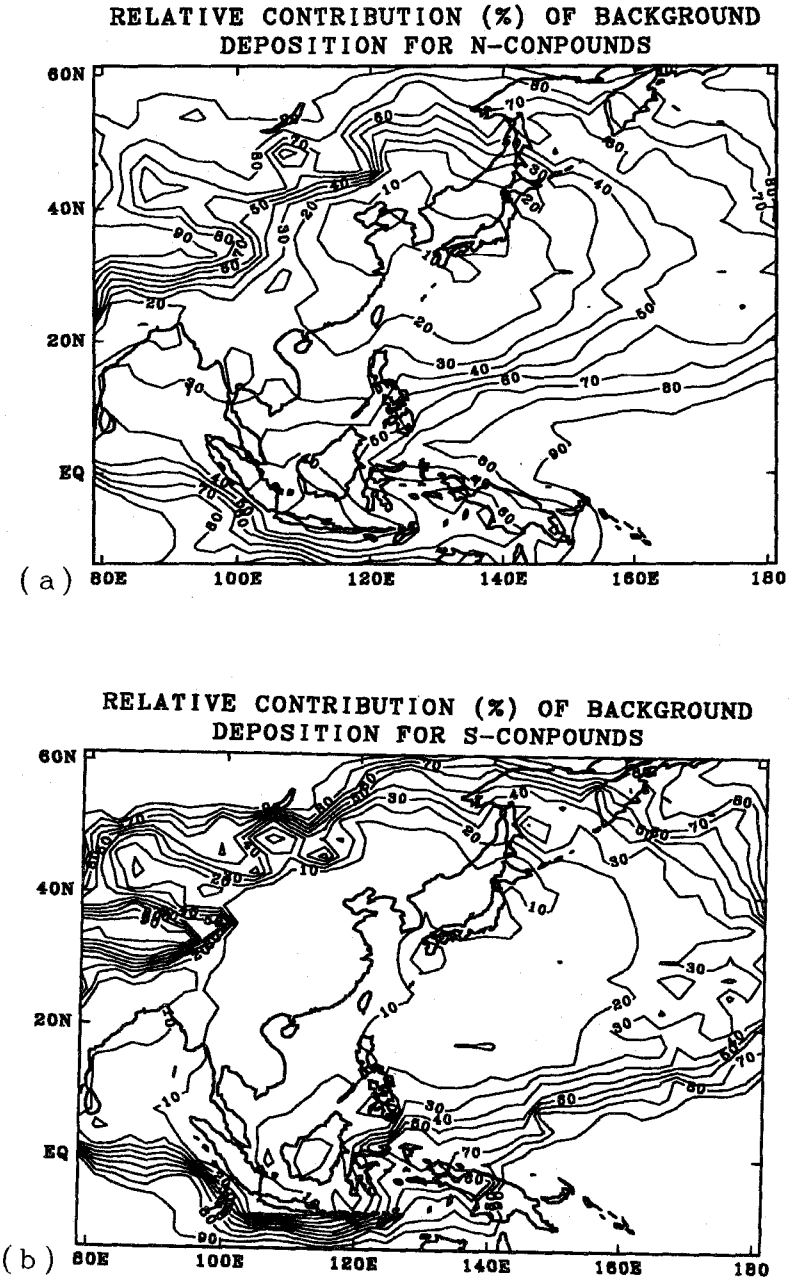

Figure 7. Ratio of background deposition (EMI_BACK in Table 2) to total deposition (BASE) in % : (a) N- and (b) S-deposition.

onto deposit-gauge under no-precipitation condition. Chemical analysis of the accumulated wet deposition was carried out every two weeks, and similarly, that of the soluble components in the accumulated dry deposition was done every one month. This method for dry deposition implies that the observed value may not represent the dry deposition onto real earth's surface because of artificial turbulence generated by the sampling apparatus and the chemical nature of the artificial surface differing from the natural one. Precise comparison between pbserved and simulation-derived dry-depositions may not be realistic due to uncertainties included in the observation and the simulation in which simple surface type is usually assumed for a large grid cell. Since the observed data were given in monthly value, they were linearly interpolated to those for 14 days. Figures 8a through f compare the calculated versus observed S- and N-depositions in the base case (Table 2) and Fig. 8g does the simulation-used- and observed-precipitations at 25 observation points, the locations of which are shown in Fig. 9: Figs. 8a , b, and c illustrate the total(*i.e.* dry + wet), dry-only, and wet-only depositions for S-compounds (*i.e.* SO_2 and SO_4^{2-}), respectively, and similarly Figs. 8d, e, and f for N-compounds (*i.e.* HNO_3 (NO_3^-) for Fig. 8f, and NO_2, HNO_3 (NO_3^-), and PAN for Figs. 8d and e). Figure 10 plots the calculated depositions against the observed, using the same data as in Fig. 8. Estimated depositions can be affected by various factors such as model parameters used for dry and wet removal processes, meteorolgical data such as precipitation, and spatial resolution of the model. In the present calculation, a number of uncertainty factors were possibly involved. Among the uncertainty factors, aside from the model parameters on which we will discuss in next subsection, most serious effect was caused probably by the coarse spatial resolution adopted in this simulation; the grid sizes $2.5° \times 2.5°$ correspond to the meridional distance of 278 km and, for example, to the zonal distance of 213 km at 40°N. Figure 9 illustrates how $2.5° \times 2.5°$ grid system accomodates the 25 observation points; in Fig. 8, for example, the points C (Sendai), D (Eno-dake), and L (Niigata) are in the same grid cell. Coarse spatial resolution forces to specify one surface type and to choose one meteorological parameter for broad area, which can introduce uncertainty into the calculated depositions. Probably most adverse effect to the correct estimation of depositions arises from too coarse approximation for emission source distribution within a grid cell. For example, the observation points I(Ichihara), J(Tokyo), K(Kawasaki), E(Kashima), and F(Tsukuba) are located in the same grid cell. Thus, only one emission source strength averaged over the cell was assigned for the simulations in spite of the well-known complex structures in emission sources in metropolitan Tokyo and its surrounding area. That the calculation-derived depositions at E(Kashima) and F(Tsukuba) (see Fig. 9), which are about 80 km to the northeast of metropolitan Tokyo, tend to go far from the 45 degree line in Fig.10 demonstrates the effect of coarse resolution in emission source distribution. Similar example can be found in the calculated depositions at A(Sapporo) and B(Nohoro) in Figs. 8c and 10c, where the strength of local emission source in Sapporo area was smoothed out over the large grid cell and thus smaller depositions were predicted (see Figs. 8c and 10c). For reference, these places are marked with the alphabet in Fig. 10. In consideration of this limitation, however, the model performance on the estimation of N- and S-depositions in Figs. 8 and 10 may be acceptable for the simulations in semi-global and global scales.

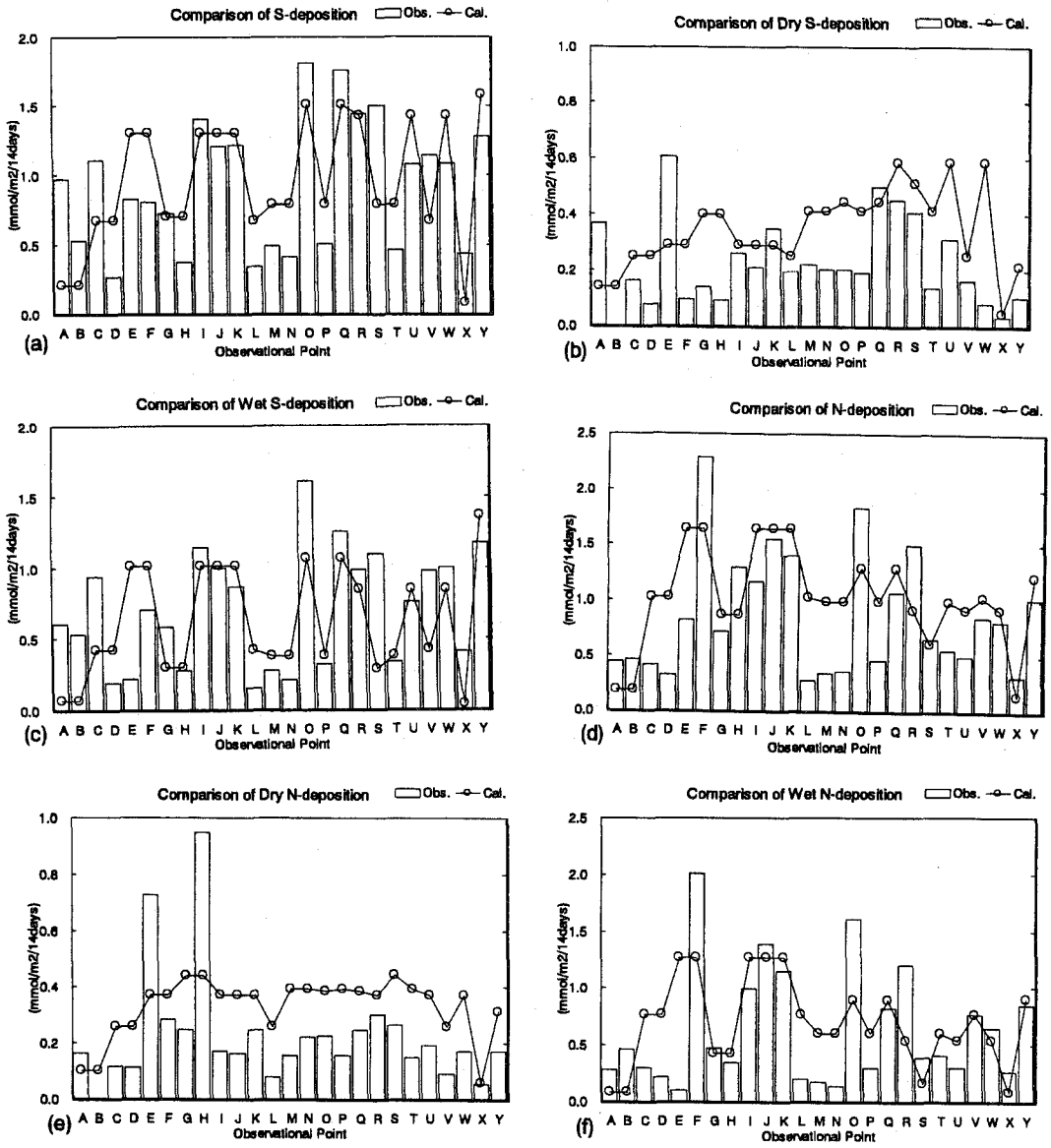

Figure 8. Comparison of the calculated deposition (BASE) with the observed at 25 points in Japan : (a) S-total-, (b) S-dry-, and (c) S-wet-depositions, where S-compounds denote SO_2 and SO_4^{2-} ; (d) N-total-, (e) N-dry-, (f) N-wet-depositions, where N-compound means HNO_3 (NO_3^-) : Fig. 8(g) shows precipitation : the observation with bar graph and the data (Xie and Arkin, 1995) used in the present simulation. Observation points : A-Sapporo, B-Nohoro, C-Sendai, D-Eno-dake, E-Kashima, F-Tsukuba, G-Nagoya, H-Inuyama, I-Ichihara, J-Tokyo, K-Kawasaki, L-Niigata, M-Osaka, N-Amagasaki, O-Matsue, P-Kurashiki, Q-Ube, R-Kitakyusyu, S-Omuta, T-Kyoto-Hachiman, U-Chikugo-Ogori, V-Sado, W-Tsushima, X-Rishiri, and Y-Amami. The locations of these points are shown in Fig. 9.

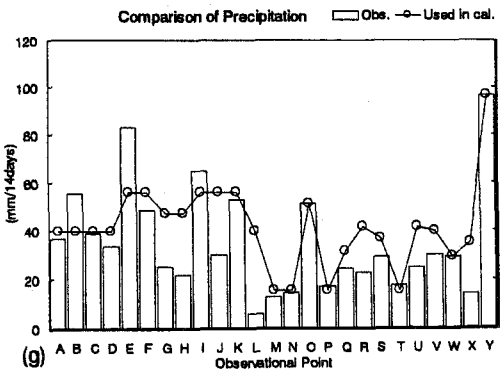

Figure 8. (Continued)

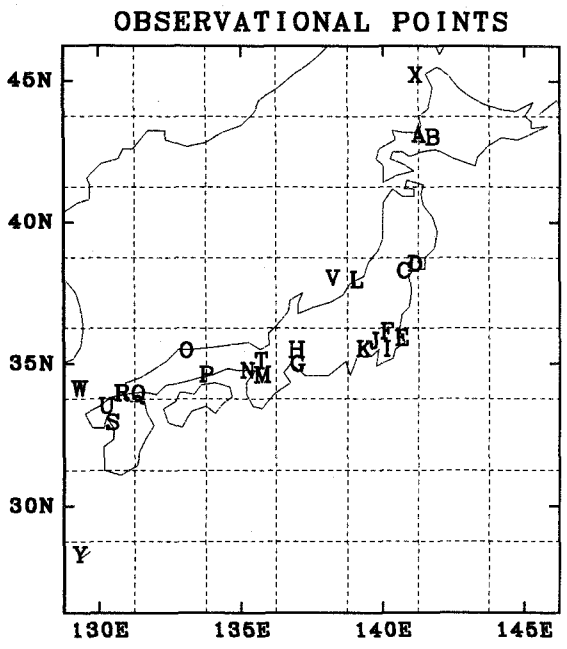

Figure 9. Observation points for acid deposition : points A through Y. One grid cell written with dashed lines expresses area of 2.5 °× 2.5 °. See also caption for Fig. 8.

4.4 Sensitivity of S-deposition over Japan to various factors

Sensitivity of depositions of sulfur compounds (i.e. SO_2 and SO_4^{2-}) over Japan area to model parameters in deposition rate formulation, and emission source distribution was investigated.

(1) Effects of pH in precipitation, aerosol capture efficiency and dry deposition velocity

Figures 11a, b, and c show effects of pH value in precipitation on total-, dry-only-, and wet-only-depositions; the results of three cases for prescribed values of pH=5.6 (base case), 5.3 (case PH5.3), or 5.0 (case PH5.0) are plotted in Fig. 11 (see Table 2 for details of the cases). The hydrogen ion concentration in precipitation could affect depositions of slfur compounds through α parameter in Eq.(6). Figure 11c suggests that by changing the prescribed pH value from 5.0 ($*$) to 5.6 ($\bigcirc$), S-wet deposition can increase by 50 %, though the effect is not necessarily same for all locations because of different temperature and also "snow-option" for scavenging that was applied in the case of the temperature at the first vertical grid being below 275 K. Figure 11b indicates inverse relation of dry deposition with the wet deposition; the reduced wet deposition is slightly recovered by the increased dry deposition (see Fig. 11a). Wet deposition process collects SO_2 and SO_4^{2-} over the depth of the atmosphere, for example, the lowest layer of 1 to 2 km, while dry deposition occurs only at the earth's surface. Thus, the dry deposition could not fully recover the decreased wet deposition. The reduced pH value in precipitation resulted in the decreases of the total S-depositions compared with BASE (pH 5.6, Table 2): reductions of 24.8 % in PH5 and 9.1 % in PH5.3 (see Table 2). The pH value in precipitation definitely varies from place to place and time to time, especially near large emission source area. Thus, it may be noted that acid deposition simulation with coarse spatial and temporal resolutions and simple modeling of the processes inherently includes some uncertainties.

Effects of aerosol capture efficiency on the wet deposition were tested by changing η_r for rain in Eq.(2) and η_s for snow in Eq.(3). Generally speaking, changing these parameters within the range described below did not bring in drastic changes in the depostions; namely, η_r: 0.5 (BASE) to 0.3 (ETAR3), and η_s: 0.002 (BASE) to 0.001 (ETAS1). For example, Fig. 12 illustrates minor decrease of S-wet depositions in ETAR3 ($*$) compare with BASE case ($\bigcirc$). Effects of changing of dry deposition velocities was briefly studied in the case DRYVE, where the dry deposition velocities for land surface were reduced from 0.5 in BASE to 0.3 cm s^{-1} for both SO_2 and HNO_3 (Table 2). By doing so, dry depositions of SO_2 and HNO_3 decreased by about 20 % at their largest as in Fig. 12c for S-depositions, while increases of wet S-depositions are illustrated in Fig.12d. As shown in Fig.12b, some of the total S-depositions show their increase and others do not. The increased total deposition indicates effects of increased sulfur in air mass that was released over China etc., and survived more due to the reduced dry deposition velocity for subsequent long range transport to Japan, though the increased S-depositions were at most by 9 % at Y, the Amami station in Fig. 9. Anyway the reduced dry deposition velocity (DRYVE in Table 2) resulted in slight increase of the total S-deposition over Japan, *i.e.* by 0.6 %, and slight decrease of the total N-depositions, *i.e.* by 2.1 %.

(2) Effects of emission sources

Emission sources themselves have possible large uncertainties. Thus, we performed several simulations to see the effects of emission source strength and distribution: BASE in Table 2 uses annually averaged values of anthropogenic NO_x and SO_x emissions, while EMI_DJF adopts the "winter" emission sources that were estimated by multiplying the annual average emissions by appropriate factors prepared in the GEIA project (1997) where the factor for NO_x was set at 1 always and everywhere, and that for SO_x was, for example, 1.2 to 1.4 over

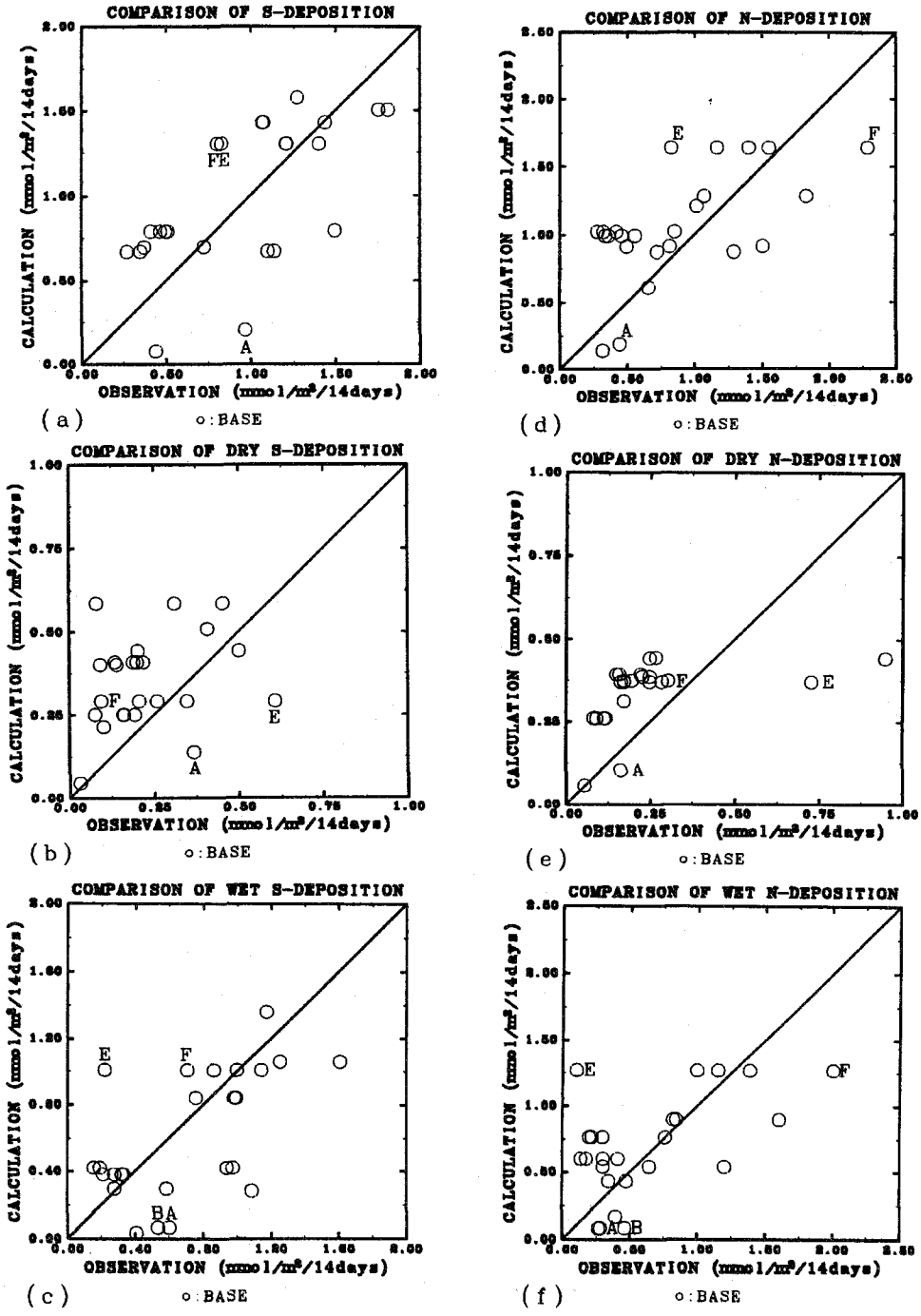

Figure 10. Calculated(BASE in Table 2) VS. observed depositions at the points A through Y in Fig. 9 : (a) S-total-, (b) S-dry-, and (c) S-wet-depositions ; similarly (d) N-total-, (e) N-dry-, and (f) N-wet-depositions. The N-wet-deposition includes that of HNO_3 (NO_3^-). The letter A indicates Sapporo, B Nohoro, E Kashima and F Tsukuba. At Nohoro (i.e. B), only wet-deposition was observed.

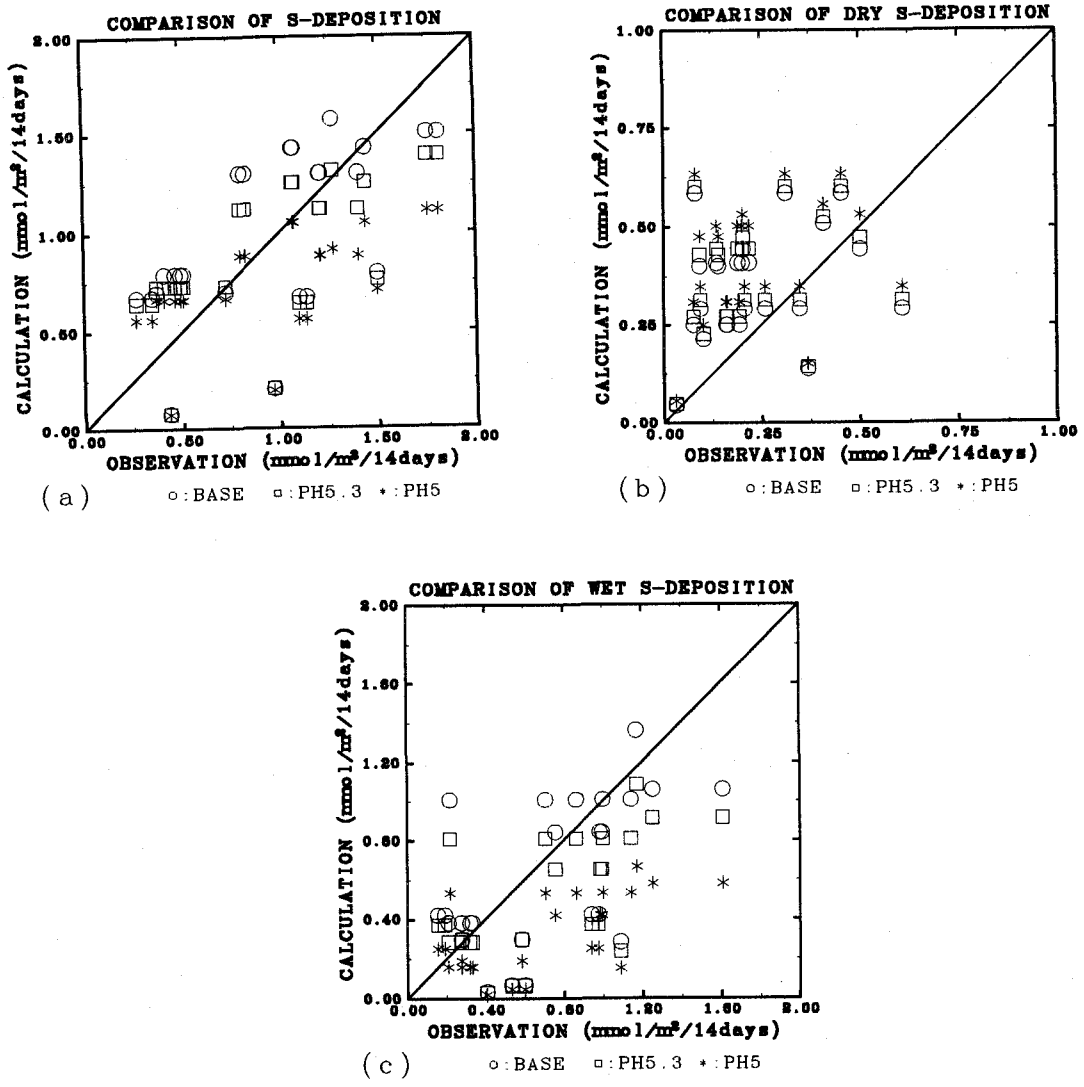

Figure 11. Calculated VS. observed S-depositions. Sensitivity of calculated S-depositions to pH in rain drop : (a) total-S-, (b) dry-S-, and (c) wet-S-depositions. The open circle, open square, and asterisk stand for the case of BASE, PH5.3, and PH5, respectively (see Table 2 for the cases).

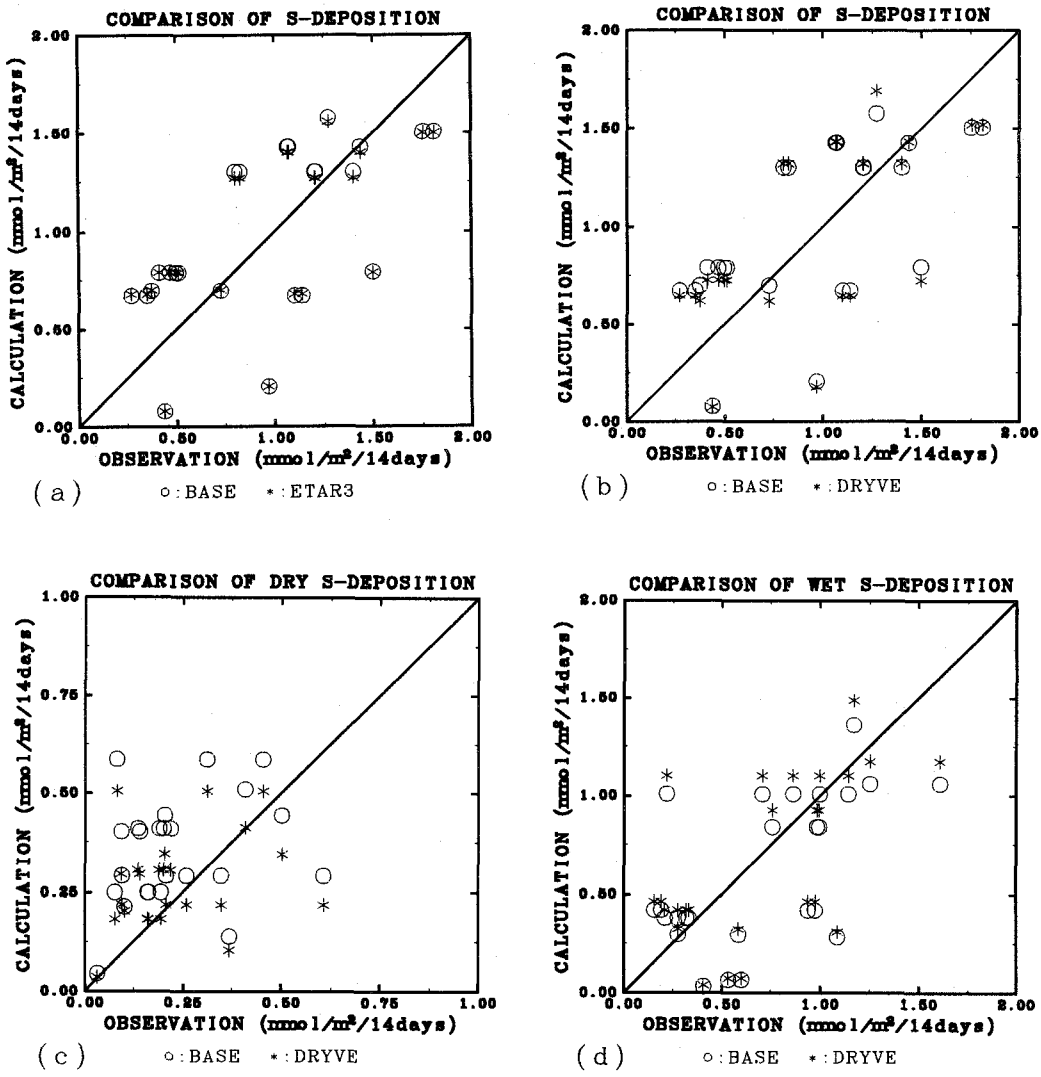

Figure 12. Effect of scavenging parameters on calculated depositions : (a) sensitivity of S-total deposition to η_r in Eq. (2), ○ for BASE and $*$ for ETAR3 ; sensitivity of (b) S-total-deposition, (c) S-dry-deposition, and (d) S-wet-deposition to dry-deposition velocities ; ○ for BASE and $*$ for DRYVE (see Table2).

Table 3. Calculated depositions over Japan area (kmol/14day).

Case	N compounds				S compounds			
	Dry			Wet	Dry		Wet	
	HNO_3	NO_2	PAN	HNO_3	SO_2	SO_4^{2-}	SO_2	SO_4^{2-}
BASE	2.86E5	0.72E5	0.06E5	5.10E5	2.37E5	0.11E5	3.73E5	1.17E5
	8.74E5‡				7.38E5‡			
EMI_DJF	2.87E5	0.72E5	0.06E5	5.10E5	2.61E5	0.16E5	4.06E5	1.30E5
	8.75E5‡				7.13E5‡			
EMI_DJF2	3.89E5	0.73E5	0.07E5	6.88E5	3.30E5	0.23E5	5.67E5	2.08E5
	11.7E5‡				11.3E5‡			
EMI_MAM	2.87E5	0.72E5	0.06E5	5.10E5	2.21E5	0.13E5	3.51E5	1.08E5
	8.75E5‡				6.93E5‡			
EMI_JPOFF	1.90E5	0.08E5	0.05E5	3.34E5	1.29E5	0.12E5	2.91E5	1.04E5
	5.37E5‡				5.36E5‡			
EMI_BACK	0.20E5	0.01E5	0.02E5	0.67E5	0.09E5	<0.01E5	0.69E5	0.08E5
	0.90E5‡				0.12E5‡			
Emission strength over Japan	15.3E5				5.50E5			

* For example, 2.86E5 denotes 2.86×10^5

‡ Sum of the deposition.

$ HNO_3 stands for HNO_3 and NO_3^-.

inland China and 1.2 in northern Japan, EMI_MAM does the "spring" emissions similarly, where the factor for SO_x was around 0.9 for China; and EMI_JPOFF uses the same emission sources as the BASE case except for no Japanese sources. The calculated depositions in various emission-scenario-related cases of N- and S-compounds over Japan area are listed in Table 3. EMI_BACK in Table 3 represents the case without any explicit emission sources except for SO_2 emission from volcano. Table 3 suggests the total S-deposition in BASE is just in between those of EMI_DJF and EMI_MAM; compared with the deposition in BASE, that in EMI_DJF is by 10 % larger and that in EMI_MAM is by 6 % less. In contrast to the S-deposition, the N-deposition including dry depositions of NO_2 and PAN does not show significant difference among those in three cases, *i.e.* BASE, EMI_DJF, and EMI_MAM (see Table 3).

4.5 Contribution of the Asian continental sources and others to acid deposition in Japan

Using the simulation results of BASE and EMI_JPOFF, the relative contributions of the emission sources in the Asian continent and other sources to acidic deposition over Japan area were evaluated, and they are presented in % in Figs. 13a and b for the total N- and S-depositions, respectively. Other sources include aircraft emission and lightning source for NO_x, and volcano for SO_x. Figure 13 shows that (1) the relative contributions are larger in western part of Japan, *e.g.* more than 70 % of N-deposition and 80 % of S-deposition in

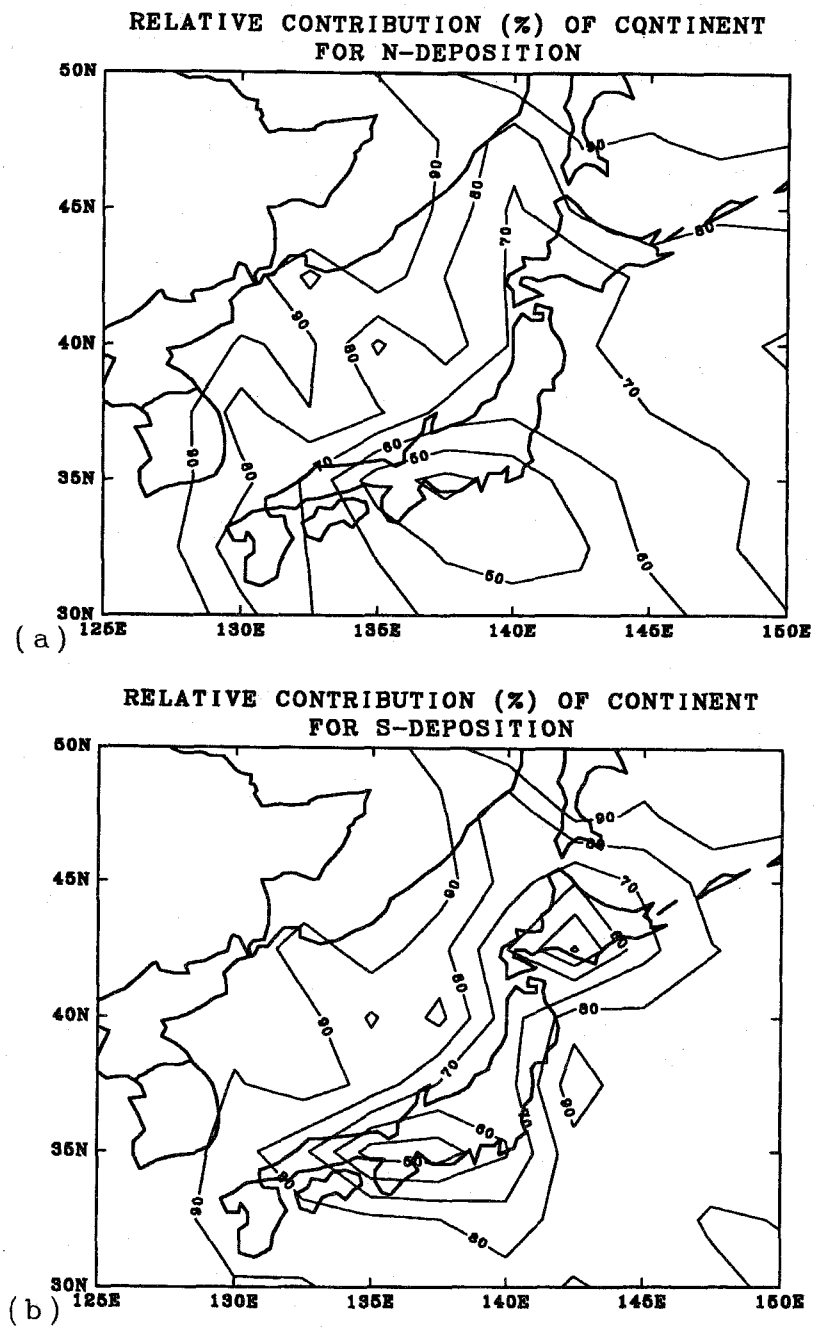

Figure 13. Calculated relative contribution of the Asian continent sources to depositions onto Japan area : (a) N-total-deposition, and (b) S-total deposition. This was derived using BASE and EMI_JPOFF results. Contour lines are drawn every 10 %.

Kyushu island, (2) in and near strong emission source area in the middle of Japan, the contributions are relatively low, *e.g.* less than 40 % for N-deposition and 50 % for S-deposition, and (3) the continental sources have larger influence on S-deposition than on N-deposition. From the results of BASE, and EMI_JPOFF in Table 3, the total contributions of the sources in thecontinent and others can be assessed as (total deposition in EMI_JPOFF)/(total deposition in BASE case): 72.6 % for S-deposition and 61.4 % for N-deposition. This lower contribution to N-deposition reflects relatively large NO_x emission in Japan and also shorter life time of HNO_3 in the atmosphere compared with SO_4^{2-}. Direct contribution of the continental NO_x sources to N-deposition over Japan may be further smaller than 60 %, since it is natural to consider that aircraft NO_x emission due to busy traffic over Japan contribute significantly.

Relative contributions of various chemical species to the dry and wet depositions of N- and S-compounds, whose horizontal distributions are shown in Figs. 5a and b, were calculated over Japan area from BASE case in Table 3 as follows: N-deposition (58.3 % by wet deposition of HNO_3, hereafter abbreviated as "wet-HNO_3", 32.8 % by dry-HNO_3, 8.2 % by dry-NO_2, and 0.7 % by dry-PAN), and S-deposition (50.6 % by wet-SO_2, 32.1 % by dry-SO_2, 15.8 % by wet-SO_4^{2-}, and 1.5 % by dry-SO_4^{2-}), where wet-SO_2 is assumed to be eventually converted to SO_4^{2-}. These ratios and the source contributions in Figs. 13a and b, of course, can vary depending on how dry and wet deposition processes are modeled. To examine the model processes related to acid deposition, it is necessary that the observed deposition data collected over not only Japan but also large Pacific rim area are compared with simulation results simultaneously.

4.6 Prediction of future acid deposition over East Asia

It is reported in USEIA (1997) that coal consumption in China will be doubled by 2010 from its 1990 basis. In this subsection how much this increase of coal consumption in China can raise acid deposition over east Asia is investigated. The simulation case EMI_DJF2 in Table 2 stands for the case in which NO_x and SO_x emissions due to fuel combustion in China are doubled with the seasonal factor for "winter". Figures 14a and b show N- and S-depositions, respectively, calculated in EMI_DJF2. Extremely high S-depositions can be seen in Suchowan Basin and Shanghai area in China, and also high N-deposition in Shanghai area. Figures 15a and b illustrate increase of N- and S-depositions (%), respectively, from those of EMI_DJF, which is assumed to be representative of 1990 situation. Figure 15 demonstrates that (1) S-depositions could be increased by 90 %, and N-depositions by 80 % for almost whole China, and (2) S-depositions in Japan could be increased by more than 40 %, and N-depositions by more than 30 %. These all suggest that serious damage to the eco-systems in east Asia may take place in near future when no counter action would be taken.

5. Summary and Conclusions

Long range transport/transformation/deposition of various trace chemical species has been simulated over east- and southeast-Asia and the west Pacific ocean during February and March, 1994, and the results for March, 1994 were analyzed. The simulations included natural emission sources of NO_x due to lightning, soil microbial activity and biomass-burning, and of SO_x from volcano as well as anthropogenic sources of NO_x, SO_x and hydrocarbons; the anthropogenic NO_x sources also included aircraft emissions. Comparison of calculated concentrations with PEM-West-B (Pacific Exploratory Mission-West, Phase B) campaign data (*e.g.*, Kondo *et al.*, 1997) showed good agreement for O_3, CO, SO_2 and hydrocarbons such as C_2H_4, C_2H_6 and

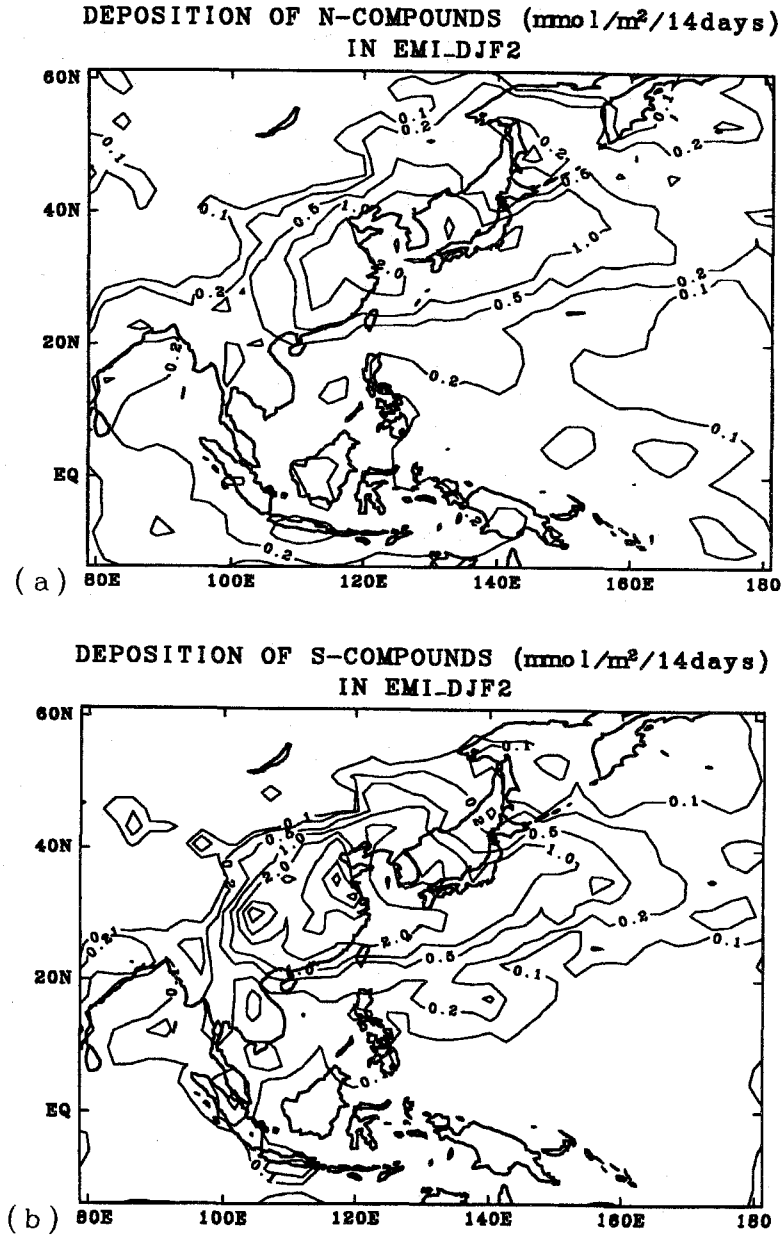

Figure 14. Calculated depositions in EMI_DJF2, i.e. doubled emissions in China for 2010 : (a) total-N-deposition and (b) total-S-deposition. Contour lines : 0.1, 0.2, 0.5, 1.0, 2.0, 4.0, and 6.0 mmol m^{-2} $(14day)^{-1}$.

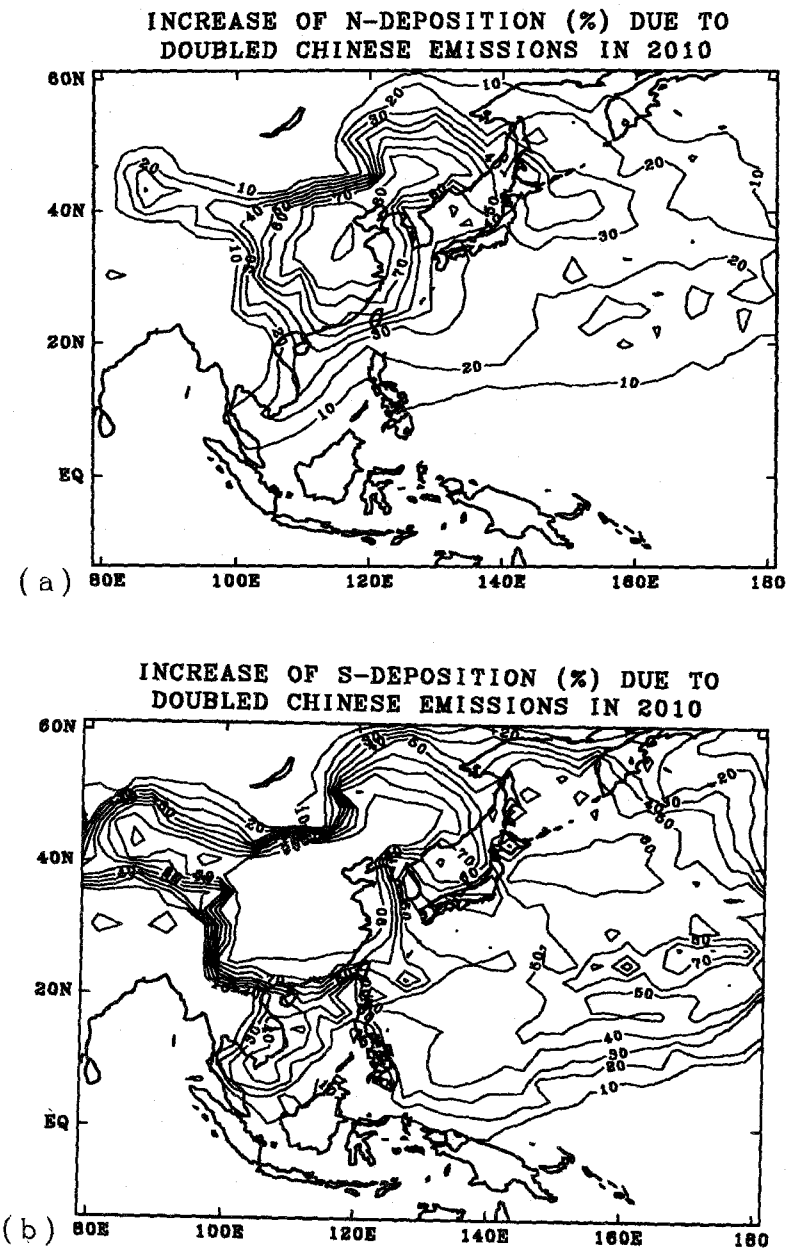

Figure 15. Evaluated increase in % of depositions from EMI_DJF case in 1990 to EMI_DJF2 case in 2010 : (a) N-total-, and (b) S-total-depositions. Contour lines are drawn every 10 %.

C_3H_8, and acceptable agreement for NO_x, HNO_3 and PAN. Furthermore, dry and wet depositions of both S- and N-compounds were calculated and the results were discussed in terms of sensitivity to model parameters, relative contributions of sources in the Asia continent and others to the depositions in Japan area, and so on.

Obtained results are summarized as follows:

(1) The "BASE" simulation in Table 2 well reproduced concentartions of various key chemical species observed during PEM-West-B campaign, and also showed acceptable agreement between the calculated and the observed depositions of N- and S-compounds over Japan area; here N-compounds for HNO_3 (NO_3^-) and S-compounds for SO_2 and SO_4^{2-}.

(2) It was suggested that depositions of N-compounds in the tropical southeast Asia may be significantly influenced by NO_x produced by lightning, soil microbial activity, and biomass-burning.

(3) Sensitivity test demonstrated that pH value in rain drop can largely affect wet S-deposition, for example, the change of pH from 5.6 to 5.0 could reduce S-deposition by as much as 20 %, indicating that one should be careful in determination of pH values in large scale models, in which to explicitly express transport of chemical species in rain and cloud phases is often difficult.

(4) Aerosol capture efficiencies η_r in Eq.(2) and η_s in Eq.(3) showed rather small effects on the depositions for the range of variation adopted in the study, *i.e.* $0.3 \leq \eta_r \leq 0.5$ and $0.001 \leq \eta_s \leq 0.002$.

(5) Change of dry deposition velocity affects, of course, dry deposition itself, but not so much for total(*i.e.* dry + wet) deposition since wet deposition tends to compensate the change occured in dry deposition especially in and near emission source area.

(6) S- and N-depositions over Japan area in early March could have large contribution from the sources in the Asia continent and others such as aircraft NO_x emission ; BASE case suggests that 72.6 % of S-depositions and 61.4 % of N-depositions over Japan can be due to the material transported from the continent and others.

(7) Based on the predicted coal consumption in China in 2010 which is about twice of that in 1990, a simulation case using doubled emissions in China was performed, and the results suggest that compared with 1990 situation, S- and N-depositions can increase by 90 % and 80 %, respectively, over almost whole China; S- and N-depositions over Japan would be raised by 40 % and 30 %, respectively.

Acknowledgments

This work was supported in part by the Environmental Agency of Japan through the research grant for "Modeling of Acid Rain Transport in East Asia" within the Global Environment Research Fund.

References

Akimoto, H., and H. Narita, 1994: Distribution of SO_2, NO_x and CO_2 emissions from fuel combustion and industrial activities in Asia with 1° x 1° resolution. *Atmos. Environ.*, Vol. 28, pp. 213-225.

Bruijnzeel, I.A., 1989: *J. Tropical Ecology*, Vol.5, pp. 187-202.

Fishman, J., and Crutzen, P., J., 1978: The origin of ozone in the troposphere. *Nature*, Vol. 274, pp. 855-858.

GEIA, 1997: GEIA Data Management and Communication Center, 1997, Data downloaded from the homepage.

Gillett, R.W., Ayers, G.P., Ginting, N., Selleck, P., and Tapper, N., 1992: *Summary Document of 2nd IGAC CAAP(Chemistry and Acidity of Asian Precipitation) Workshop*, 30th September-2nd October, 1992, Bombay, India.

Ikeda, Y., and Higashino, H., 1997: The estimation of acid deposition in East Asia (II) - Focused on the ratio of sources contribution of the deposition. *J. Japan Society for Atmos. Environ.*, Vol. 32, 175-186 (in Japanese).

Kitada, T., 1987: Turbulence structure of sea breeze front and its implication in air pollution transport - Application of $k - \epsilon$ turbulence model. *Boundary-Layer Meteor.*, Vol. 41, pp. 217-239.

Kitada, T., 1994: Transport, transformation, and deposition model for acid rain. *Meteorological Research Notes*, No.182, pp.95-118 (in Japanese).

Kitada, T., Isogawa, S., and Kondo, Y., 1996: Long range transport of NO_x, SO_x and O_3 over east Asia and the northern Pacific ocean caused by typhoons. *Air Pollution Modelling and Its Application XI*, Plenum Pub. Co., pp. 191-201.

Kitada, T., and Lee, P.C.-S., 1993: Numerical modeling of long-range transport of acidic species in association with meso- β -convective clouds across the Japan sea resulting in acid snow over coastal Japan -II. Results and discussion. *Atmos. Environ.*, Vol. 27A, pp. 1077-1090.

Kitada, T., Lee, P.C.-S., and Ueda, H., 1993: Numerical modeling of long-range transport of acidic species in association with meso- β -convective clouds across the Japan sea resulting in acid snow over coastal Japan -I. Model description and qualitative verifications. *Atmos. Environ.*, Vol. 27A, pp. 1061-1076.

Kitada, T., Nishizawa, M., and Kondo, Y., 1998: Long range transport of NO_x, NO_y, O_3 and SO_x over East Asia and the western Pacific ocean in winter season -A numerical analysis. *Air Pollution Modelling and Its Application XII*, Plenum Pub. Co., in press.

Kitada, T., Okamura, K., and Tanaka, S., 1998: Effects of topography and urbanization on local winds and thermal environment in Nohbi plain, coastal region of central Japan -A numerical analysis by meso-scale meteorological model with k- ε turbulence model. *J. Appl. Meteor.*, Vol. 37, in press.

Kondo, Y., Koike, M., Kawakami, S., Singh, H. B., Nakajima, H., Gregory, G. L., Blake, D. R., Sachse, G. W., Merrill, J. T., and Newell, R. E., 1997: Profiles and partitioning of reactive nitrogen over the Pacific Ocean in winter and early spring. *J. Geophys. Res.*, Vol. 102, pp. 28,405-28,424.

Knutson, E. O., and Stockham, J.D., 1976: Aerosol collection by snow and ice crystals. *Atmos. Environ.*, Vol. 10, pp. 395-402.

Kumar, P.P., Manohar, G.K., and Kandalgaonkar, S.S., 1995: Global distribution of nitric oxide produced by lightning and its seasonal variation. *J. Geophys. Res.*, Vol. 100, pp. 11,203-11,208.

Lurmann, F.W., Lloyd, A.C., and Atkinson, R., 1986: A chemical mechanism for use in long-range transport/acid deposition computer modeling. *J. Geophys. Res.*, Vol. 91, pp. 10,905-10,936.

Matsuoka, Y, 1992: Future projection of global anthropogenic sulfur emission and its environmental effect. *Environmental Systems Research*, Vol.20, pp. 142-151(in Japanese).

Murao, N., Ohta, S., Yamagata, S., and Mizoguchi, I., 1993: The impact of emission from Sakurajima volcano on acid deposition in Japan. *Proc. 1st Global Environmental Symposium*, pp. 183-188 (in Japanese).

Nakanishi, H., 1996: Emission sources and concentrations of non-methane hydrocarbons over the Nohbi plain in central Japan. *Toyohashi Univ. Technology, B.S. thesis*, 42p. (in Japanese).

NASA Langley, 1997: Archive on aircraft emissions in 1990.

Slinn, W.G.N., 1974: Dry deposition and resuspension of aerosol particles—a new look at some old problems. In R.J. Engelmann and G.A. Sehmel (coord.) *Atmosphere-Surface Exchange of Particulate and Gaseous Pollutants*, pp. 1-40. Avail. NTIS, Springfield, Virginia as CONF-740921.

Slinn, W.G.N., 1974: Some approximations for the wet and dry removal of particles and gases from the atmosphere. *Water, Air, and Soil Poll.*, Vol. 7, pp. 513-543.

Strand, A., and Hov, O., 1993: A two-dimensional zonally averaged transport model including convective motions and a new strategy for the numerical solution. *J. Geophys. Res.*, Vol. 98, pp. 9023-9037.

Suurikeikaku Co. Ltd., 1995: *Acid Rain Monitoring and Data Analysis for 1993-1994, Report to the Environmental Agency of Japan*, 366p.(in Japanese).

USEIA, 1997: United States Energy Information Administration. Data downloaded from the homepage.

Washington, W.M., and Williamson, D.L., 1977: A description of the NCAR global circulation models. In *Methods in Computational Physics, Vol. 17: General Circulation Models of the Atmosphere*,Academic Press, pp.111-265.

Xie, P., and Arkin, P.A., 1995: An intercomparison of gauge observations and satellite estimates of monthly precipitation. *J. Appl. Meteor.*, Vol. 34, pp. 1143-1160.

Yienger, J.J., and Levy II, H., 1995: Empirical model of global soil-biogenic NO_x emissions. *J. Geophys. Res.*, Vol. 100, pp. 11,447-11,464.